The Astrophysical Journal, 834:166 (6pp), 2017 January 10 doi:10.3847/1538-4357/834/2/166

REVISITING A CLASSIC: THE PARKER–MOFFATT PROBLEM

O. Pezzi[1], T. N. Parashar[2], S. Servidio[1], F. Valentini[1], C. L. Vásconez[3], Y. Yang[2], F. Malara[1], W. H. Matthaeus[2], and P. Veltri[1]
[1] Dipartimento di Fisica, Università della Calabria, 87036 Rende (CS), Italy
[2] Department of Physics and Astronomy, University of Delaware, DE 19716, USA
[3] Departamento de Física, Escuela Politécnica Nacional, Quito, Ecuador
Received 2016 September 14; revised 2016 November 15; accepted 2016 November 23; published 2017 January 11

ABSTRACT

The interaction of two colliding Alfvén wave packets is described here by means of magnetohydrodynamics (MHD) and hybrid kinetic numerical simulations. The MHD evolution revisits the theoretical insights described by Moffatt, Parker, Kraichnan, Chandrasekhar, and Elsässer in which the oppositely propagating large-amplitude wave packets interact for a finite time, initiating turbulence. However, the extension to include compressive and kinetic effects, while maintaining the gross characteristics of the simpler classic formulation, also reveals intriguing features that go beyond the pure MHD treatment.

Key words: magnetohydrodynamics (MHD) – plasmas – solar wind

1. INTRODUCTION

A familiar perspective on the hydromagnetic description of astrophysical and laboratory plasma turbulence begins with the interaction of oppositely propagating large-amplitude incompressible wave packets (Iroshnikov 1964; Kraichnan 1965). Various nonlinear phenomenologies are built on this paradigm (Dobrowolny et al. 1980a; Velli et al. 1989; Ng & Bhattacharjee 1996; Matthaeus et al. 1999; Galtier et al. 2000; Verdini et al. 2009). An essential feature is that large-amplitude perturbations in which fluctuations in velocity $\boldsymbol{u}$ and magnetic field $\boldsymbol{b}$ are Alfvénically correlated, i.e., either $\boldsymbol{u} = (c_A/B_0)\boldsymbol{b}$ or $\boldsymbol{u} = -(c_A/B_0)\boldsymbol{b}$ (where c_A and B_0 are uniform background Alfvén velocity and magnetic field, respectively), are exact stable solutions to the equations of incompressible magnetohydrodynamics (MHD) (Elsässer 1950; Chandrasekhar 1956). One thread emerging from this concerns the analysis of colliding wave packets to reveal properties of the spectrum of MHD turbulence (Kraichnan 1965).

A different emphasis was given by Moffatt (1978) and Parker (1979). Both of these treatments analyzed the collision of large-amplitude incompressible, ideal Alfvén wave packets, noting that nonlinear interaction and mutual distortion of the wave packets are limited to the span of time during which they spatially overlap. Both Moffatt and Parker argued (somewhat differently, as discussed later) that the packets eventually separate and propagate once again undisturbed without further interactions. This paper addresses two questions that arise when trying to apply this physical insight to high-temperature extraterrestrial plasmas such as the solar wind, where such large-amplitude Alfvénic fluctuations are routinely observed (Belcher & Davis 1971), or the solar corona, where the interaction of Alfvénic wave packets is thought to occur (Matthaeus et al. 1999). First, both compressibility effects and kinetic plasma are likely to be important in space applications, and we ask whether these give rise to significant departures from the Parker–Moffatt scenario. Second, we ask whether the proposed separation of the packets after collision is realized as envisioned or whether a wake of non-propagating disturbances might remain after very long times. We address these specific questions using a compressible MHD model and a hybrid Vlasov model. Broader questions that emerge will be discussed in the concluding remarks.

In dealing with fluids and MHD models of quasi-incompressible, low Mach number flows, either in numerical simulations (Orszag 1971; Orszag & Patterson 1972; Kraichnan & Montgomery 1980), in applications (Dobrowolny et al. 1980b; Matthaeus et al. 1999), or in analytical theory (Orszag 1977; Oughton et al. 2006), one routinely deals with two significant properties: first, the dominant quadratic couplings are of the form $\boldsymbol{k} = \boldsymbol{p} + \boldsymbol{q}$, transferring energy into (or from) a Fourier mode with wavevector $\boldsymbol{k}$ due to nonlinear interactions with modes with wavevectors $\boldsymbol{p}$ and $\boldsymbol{q}$. One concludes that in general (unless, e.g., all excited wavevectors are collinear) one expects excitations to spread rapidly among many wavevectors, a process that over time can produce complex mixing and turbulent flows. Second, incompressible MHD nonlinear evolution proceeds as $\partial z_i^+/\partial t \sim -z_j^- \nabla_j z_i^+$ and $\partial z_i^-/\partial t \sim -z_j^+ \nabla_j z_i^-$ in terms of Elsässer variables $z_j^\pm = u_j \pm b_j$ (jth components of velocity field u_j and magnetic field b_j in units of the Alfvén speed), thus allowing the immediate conclusion that nonlinear couplings vanish unless the Elsässer fields $\boldsymbol{z}^+$ and $\boldsymbol{z}^-$ have nonzero overlap somewhere in space. These properties not only provide motivation for the problem of collision of Alfvén wave packets, but also enter into some of its complexity as an elementary interaction that generates turbulence (Kraichnan 1965; Dobrowolny et al. 1980b; Howes & Nielson 2013; Drake et al. 2016).

Beyond the assumption of incompressibility, we may anticipate genuinely compressible and kinetic effects that warrant examination in the problem of collision of large-amplitude wave packets. In the solar wind, for example, many intervals, especially within 1 au (Bruno et al. 1985) or at high latitudes (McComas et al. 2000), are highly Alfvénic, but even within such intervals there are mixtures of Elsässer amplitudes, small density variations, and a small parallel variance, as in the well-quoted "5:4:1" variance ratio reported by Belcher & Davis (1971). There have also been reports of interaction between interplanetary magnetosonic wave packets (He et al. 2015), while the great power law in the interstellar medium (Armstrong et al. 1981) is associated with electron density fluctuations that may be either propagating or non-propagating (Zank & Matthaeus 1992). Furthermore, in plasmas such as the

solar wind, at smaller scales near the ion inertial scale, one expects kinetic properties (Alexandrova et al. 2008) such as spectral steepening (Bruno & Carbone 2013), dispersive wave effects (Sahraoui et al. 2007; Gary et al. 2010) of both kinetic Alfvén wave (KAW) and whistler types, along with temperature anisotropy, beams, and other distortions of the proton velocity distribution function (VDF) (Marsch 2006; Valentini et al. 2007, 2014; Servidio et al. 2012, 2015). These complications place the problem of collisions of Alfvén wave packets in a much more complex framework.

2. MODELS AND APPROACH

Motivated by these considerations, we revisit the problem of two colliding large-amplitude Alfvén wave packets by means of compressible fluid and kinetic Vlasov–Maxwell simulations. The results shown are from an MHD model and a hybrid kinetic plasma (HVM) model. Both retain 2.5 dimensions in the physical space, with three Cartesian fluid velocities and field components, but with gradients only in the (x, y) plane. The HVM model also has a three-dimensional grid in velocity space.

It is clear that this problem would be better addressed in a high-resolution fully 3D representation in physical space. However, computational cost limits accessible 3D simulations to relatively low spatial resolution. This present geometry is favored because it allows for a large system size, which, in turn, ensures a large Reynolds number and hence MHD-like turbulent dynamics (Parashar et al. 2015a), as well as a realistic realization of compressive fluctuations/parallel variances (Parashar et al. 2016).

The dimensionless MHD equations are

$$\partial_t \rho + \nabla \cdot (\rho \boldsymbol{u}) = 0, \tag{1}$$

$$\partial_t \boldsymbol{u} + (\boldsymbol{u} \cdot \nabla)\boldsymbol{u} = -\frac{\tilde{\beta}}{2\rho}\nabla(\rho T) + \frac{1}{\rho}[(\nabla \times \boldsymbol{B}) \times \boldsymbol{B}], \tag{2}$$

$$\partial_t \boldsymbol{B} = \nabla \times (\boldsymbol{u} \times \boldsymbol{B}), \tag{3}$$

$$\partial_t T + (\boldsymbol{u} \cdot \nabla)T + (\gamma - 1)T(\nabla \cdot \boldsymbol{u}) = 0. \tag{4}$$

In Equations (1)–(4) spatial coordinates $\boldsymbol{x} = (x, y)$ and time t are respectively normalized to $\tilde{L}$ and $\tilde{t}_A = \tilde{L}/\tilde{c}_A$. The magnetic field $\boldsymbol{B} = \boldsymbol{B}_0 + \boldsymbol{b}$ is scaled to the typical magnetic field $\tilde{B}$, while mass density ρ, fluid velocity $\boldsymbol{u}$, temperature T, and pressure $p = \rho T$ are scaled to typical values $\tilde{\rho}$, $\tilde{c}_A = \tilde{B}/(4\pi\tilde{\rho})^{1/2}$, $\tilde{T}$, and $\tilde{p} = 2\kappa_B \tilde{\rho}\tilde{T}/m_p$ (κ_B being the Boltzmann constant and m_p the proton mass), respectively. Moreover, $\tilde{\beta} = \tilde{p}/(\tilde{B}^2/8\pi)$ is a typical value for the kinetic to magnetic pressure ratio; $\gamma = 5/3$ is the adiabatic index. Details about the numerical algorithm can be found in Vásconez et al. (2015) and Pucci et al. (2016).

The kinetic simulations solve the system of hybrid Vlasov–Maxwell equations (Valentini et al. 2007) in which the proton distribution function is numerically evolved while electrons are a massless Maxwellian, isothermal fluid. Dimensionless HVM equations are

$$\partial_t f + \boldsymbol{v} \cdot \nabla f + \frac{1}{\tilde{\epsilon}}(\boldsymbol{E} + \boldsymbol{v} \times \boldsymbol{B}) \cdot \nabla_{\boldsymbol{v}} f = 0, \tag{5}$$

$$\begin{aligned} \mathbf{E} - \frac{m_e \tilde{\epsilon}^2}{m_p}\Delta \mathbf{E} &= -\boldsymbol{u_e} \times \mathbf{B} - \frac{\tilde{\epsilon}\tilde{\beta}}{2n}\left(\nabla P_e - \frac{m_e}{m_p}\nabla \cdot \Pi\right) \\ &\quad + \frac{m_e}{m_p}\left[\boldsymbol{u} \times \mathbf{B} + \frac{\tilde{\epsilon}}{n}\nabla \cdot \left(n(\boldsymbol{uu} - \boldsymbol{u_e u_e})\right)\right] \end{aligned} \tag{6}$$

$$\frac{\partial \boldsymbol{B}}{\partial t} = -\nabla \times \boldsymbol{E}; \quad \nabla \times \boldsymbol{B} = \boldsymbol{j} \tag{7}$$

where $f = f(\boldsymbol{x}, \boldsymbol{v}, t)$ is the proton distribution function. In Equations (5)–(7), velocities $\boldsymbol{v}$ are scaled to the Alfvén speed $\tilde{c}_A$, while the proton number density $n = \int f\, d^3v$ and the proton bulk velocity $\boldsymbol{u} = n^{-1}\int \boldsymbol{v} f\, d^3v$, obtained as moments of the distribution function, are normalized to $\tilde{n} = \tilde{\rho}/m_p$ and $\tilde{c}_A$, respectively. The electric field $\boldsymbol{E}$, the current density $\boldsymbol{j} = \boldsymbol{\nabla} \times \boldsymbol{B}$, and the electron pressure P_e are scaled to $\tilde{E} = (\tilde{c}_A \tilde{B})/c$, $\tilde{j} = c\tilde{B}/(4\pi\tilde{L})$, and $\tilde{p}$, respectively. Moreover $\boldsymbol{u}_e = \boldsymbol{u} - \tilde{\epsilon}\boldsymbol{j}/n$ and the parameter $\tilde{\epsilon} = \tilde{d}_p/\tilde{L}$, where $\tilde{d}_p = \tilde{c}_A/\tilde{\Omega}_{cp}$ is the proton skin depth, allows a comparison of fluid and kinetic scales. To prevent numerical instabilities, electron inertia effects have been considered in Ohm's law ($m_e/m_p = 0.01$), while, no external resistivity η is introduced. A detailed description of the HVM algorithm can be found in Valentini et al. (2007), Vásconez et al. (2015), and Servidio et al. (2015).

The simulations are set up as follows. The spatial domain $D(x, y) = [0, 8\pi] \times [0, 2\pi]$ has been discretized with $(N_x, N_y) = (1024, 256)$ mesh points, thus implying $\Delta x = \Delta y$ and also an anisotropic wavevector space. Spatial boundary conditions are periodic. In the HVM run, we adopted a uniform grid in velocity space with 51 points in each direction, in the region $v_i = [-v_{\max}, v_{\max}]$, where $v_{\max} = 2.5\tilde{c}_A$. Boundary conditions for the velocity domain assume $f = 0$ for $|v_i| > v_{\max}$ $(i = x, y, z)$. In our simulation we set $\beta_p = 2v_{\mathrm{th},p}^2/\tilde{c}_A^2 = \tilde{\beta}/2 = 0.5$, which corresponds to $v_{\max} = 5v_{\mathrm{th},p}$, and $\tilde{\epsilon} = 9.8 \times 10^{-2}$. The background magnetic field is mainly perpendicular to the x–y plane, indeed $\boldsymbol{B}_0 = B_0(\sin\vartheta, 0, \cos\vartheta)$, where the angle between $\boldsymbol{B}_0$ and the z axis is $\vartheta = 6°$.

We impose large-amplitude perturbations of the magnetic field $\boldsymbol{b}$ and bulk velocity $\boldsymbol{u}$. Density perturbations are not imposed, which implies nonzero total pressure fluctuations. In the HVM case, the proton VDF is initially Maxwellian at each spatial point. Initial perturbations consist of two Alfvénic wave packets with opposite correlation between velocity and magnetic field, separated along x. Because $B_{0,x} \neq 0$, the packets counterpropagate. The nominal time for the collision, which has been evaluated from the center of each wave packet, is about $\tau \simeq 58.9$.

The magnetic field perturbation $\boldsymbol{b}$ has been created by initializing energy in the first four wavenumbers in the y direction while, due to the x spatial localization (enforced by projection), many wavenumbers along x are excited initially. Then, a small $b_z(x, y)$ component has been introduced in such a way that the transverse condition, $\boldsymbol{B}_0 \cdot \boldsymbol{b} = 0$, holds at each domain point. Finally, the velocity field perturbation $\boldsymbol{u}$ is generated by imposing that $\boldsymbol{u}$ and $\boldsymbol{b}$ are correlated (anticorrelated) for the wave packet that moves against (along) the

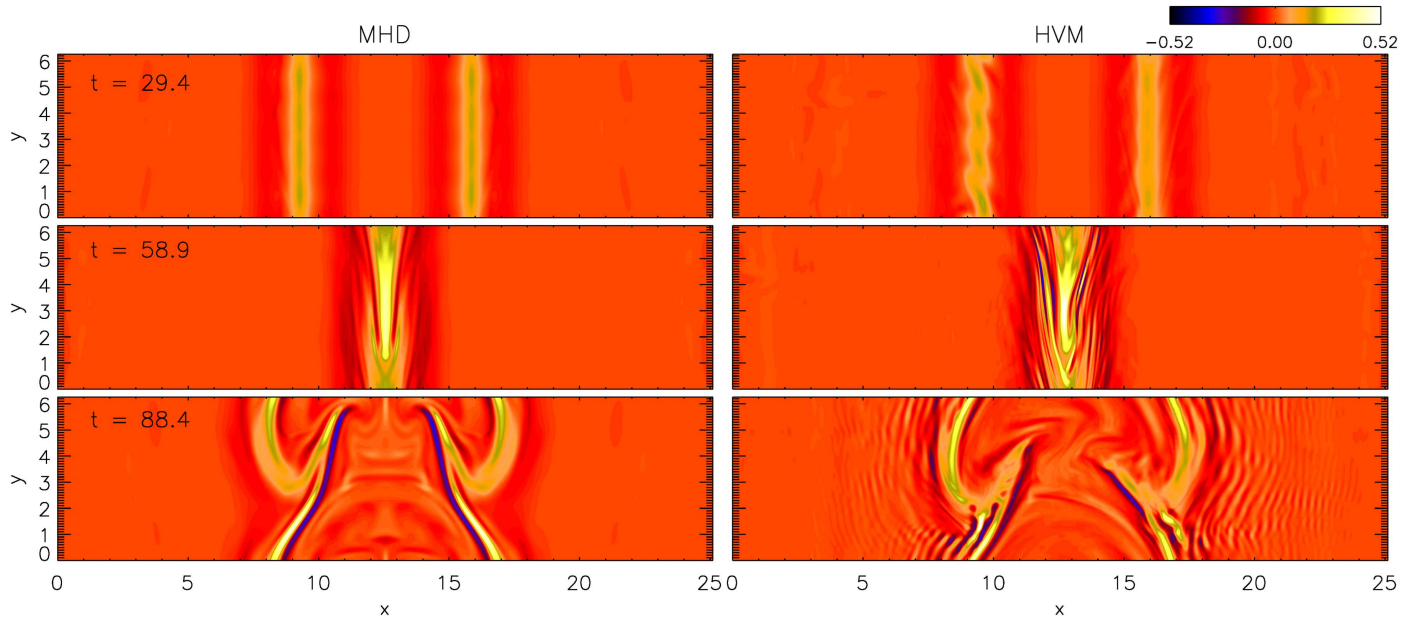

Figure 1. Contour plots of the current density $j_z(x, y)$ for the MHD (left) and the HVM (right) simulations. Top, center, and bottom rows correspond respectively to the time instants $t = 29.4$, $t = \tau = 58.9$, and $t = 88.4$.

magnetic field B_{0x}. The intensity of the perturbation is $\langle b \rangle_{\rm rms}/B_0 = 0.2$, therefore the Mach number is $M_s = \langle u \rangle_{\rm rms}/v_{{\rm th},p} = 0.4$. The intensity of fluctuations with respect to the in-plane field B_{0x} is quite strong, with a value of about 2. It is worth noting that the inverse of the intensity of the fluctuations with respect to the in-plane magnetic field is related to the parameter $\tau_{nl}/\tau_{\rm coll}$, where τ_{nl} is the characteristic nonlinear time and $\tau_{\rm coll}$ is the characteristic collision time. If $\tau_{nl}/\tau_{\rm coll} \lesssim 1$, several nonlinear times occur in a single collision and wave packets can be significantly perturbed by nonlinear effects. On the other hand, if $\tau_{nl}/\tau_{\rm coll} > 1$, many collisions are necessary to strongly distort wave packets. By evaluating $\tau_{nl} \simeq \Delta/u$ (wave packet width Δ, perturbation amplitude u) and $\tau_{\rm coll} \simeq \Delta/V$ (in-plane Alfvén propagation speed $V \simeq 0.1 c_A$), it turns out that $\tau_{nl}/\tau_{\rm coll} \simeq 0.5$. Therefore our simulations fall in a parameter range where nonlinear effects can be important to the extent that a scenario of strong turbulence may be present.

2.1. Discussion of the Initial Conditions

The imposed initial perturbations correspond to two large-amplitude Alfvén wave packets in the sense that magnetic and velocity perturbations are fully correlated in each packet, and the packets are separated in space. With zero density variation, a weak in-plane uniform magnetic field, and a relatively strong out-of-plane uniform magnetic field, this initial condition is one for which the reasoning of Moffatt and Parker discussed above would be applicable in the context of an incompressible model.

In addition, the initial data also exactly satisfy the transversality condition $\boldsymbol{B}_0 \cdot \boldsymbol{b} = 0$, which in linear compressible MHD would correspond to the Alfvén eigenmode, if indeed the amplitude were infinitesimal. Here the amplitude is large, so small-amplitude theory is unlikely to be relevant to the nonlinear evolution. Furthermore, the condition of the proper Alfvén eigenmode obtained in large-amplitude compressible MHD theory, namely $B = |\boldsymbol{B}| = $ const. is not satisfied by our initial perturbations (Barnes 1979). This suggests that pressure and density fluctuations may be generated during the evolution of the wave packets. Therefore the initial data are nonlinear eigenmodes of incompressible MHD, but not exact eigenmodes of compressible MHD. On the other hand we do not expect significant differences because the initial $B = |\boldsymbol{B}|$ fluctuations are not very large (less than 10%). Future works will analyze the evolution in the case in which $B = $ const. at $t = 0$, and in the framework of other plasma models, such as Hall MHD and particle-in-cell (PIC) kinetic plasma models.

3. NUMERICAL RESULTS

An overview of the dynamics in the two simulations (MHD and HVM) can be appreciated by inspection of the evolution of the out-of-plane component of the current density $j_z(x, y)$, reported in Figure 1. The left and right columns of Figure 1 refer to the MHD and HVM simulations, respectively. The rows refer to different instants of time: top, center, and bottom rows respectively indicate $t = 29.4$, $t = \tau = 58.9$, and $t = 88.4$. In both simulations the initially separated wave packets counterpropagate, approach each other (top panels of Figure 1), and collide at $t = \tau$. During the collision (center panels of Figure 1), j_z intensifies, and, since the overlapping wave packets interact nonlinearly, the dynamics produces small scales that can be easily appreciated by examining the width of the current structures in the center row of Figure 1. In the final stages of the simulations (bottom panels of Figure 1), the wave packets continue their motion while displaying a significantly perturbed shape. Indeed the j_z contours indicate that current structures are much more complex after the collision occurs. Moreover, their shape also exhibits a curvature that is not anticipated prior to the collision and which indicates the presence of energy in modes with gradients along the y direction, transverse to the propagation.

The MHD and HVM evolutions exhibit noticeable differences: the MHD case is symmetric with respect to $x = L_x/2 \approx 12.5$, while this symmetry is lost in the Vlasov run also before the collision (top right panel of Figure 1). The lack of the symmetry in the HVM run may be due to the

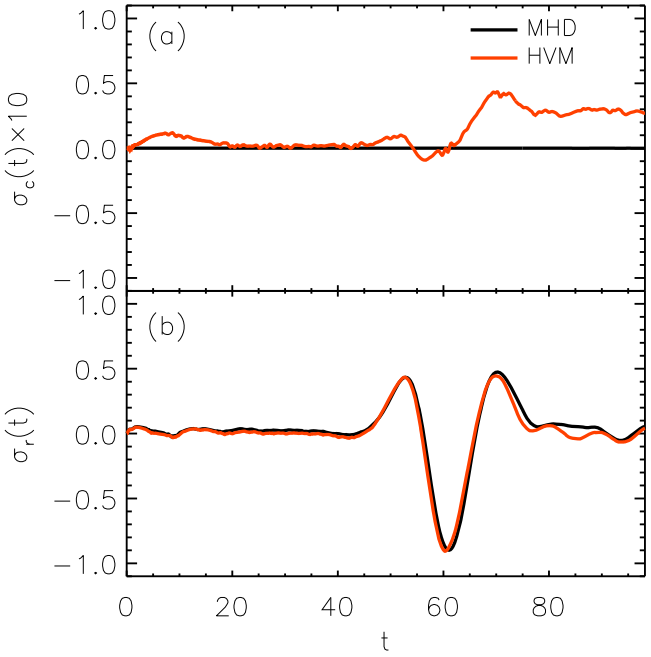

Figure 2. Temporal evolution of $\sigma_c(t)$ (a) and $\sigma_r(t)$ (b). In each panel black and red lines refer to the MHD and HVM cases, respectively.

intercoupling of B_{0x} and dispersive effects that are present in the HVM run, and may cause a different propagation along and against B_{0x}. The HVM run also forms smaller scales during the interaction than the MHD case. This difference can be appreciated in the center right panel of Figure 1. Finally, after the collision, j_z is much more complex in the HVM simulation than in the MHD run. Very thin current-sheet structures and secondary ripples are observed only in the Vlasov case. The nature of these secondary ripples may be associated with the presence of some KAW-like fluctuations (Hollweg 1999; Vásconez et al. 2015) and will be analyzed in detail in a separate paper.

A point of comparison of our simulations with the theoretical ideas given by Moffatt and Parker is to examine the behavior of cross-helicity. Those theoretical treatments assume ideal non-dissipative conditions, so that the total cross-helicity is conserved, and moreover the expectation is that the separate wave packets after the collision have the same cross-helicity as prior to the interaction. Furthermore the initial and final states, in the ideal treatment, have equipartition of flow and magnetic field energy, with departures from equipartition possible during the interaction. To examine these, Figure 2 shows the temporal evolution of (a) the normalized cross-helicity $\sigma_c(t)$ and (b) the normalized residual energy $\sigma_r(t)$ (Bruno & Carbone 2013), respectively defined as $\sigma_c = (e^+ - e^-)/(e^+ + e^-)$ and $\sigma_r = (e^u - e^b)/(e^u + e^b)$, where $e^{\pm} = \langle (\boldsymbol{z}^{\pm})^2 \rangle/2$, $e^u = \langle \boldsymbol{u}^2 \rangle/2$, $e^b = \langle \boldsymbol{b}^2 \rangle/2$, and $\boldsymbol{z}^{\pm} = \boldsymbol{u} \pm \boldsymbol{b}$.

The normalized cross-helicity $\sigma_c(t)$ is well preserved in the MHD simulation, while in the kinetic simulation it displays, around the collision time τ, a significant growth followed by a saturation stage. It is worth noting that, in the MHD run, $\sigma_c(t)$ is still conserved despite it being an invariant of the incompressible MHD yet our MHD simulation is compressible (compressibility could, in principle, break the invariance of $\sigma_c(t)$). This characteristic reflects the fact that the compressive fluctuations that are dynamically generated during the

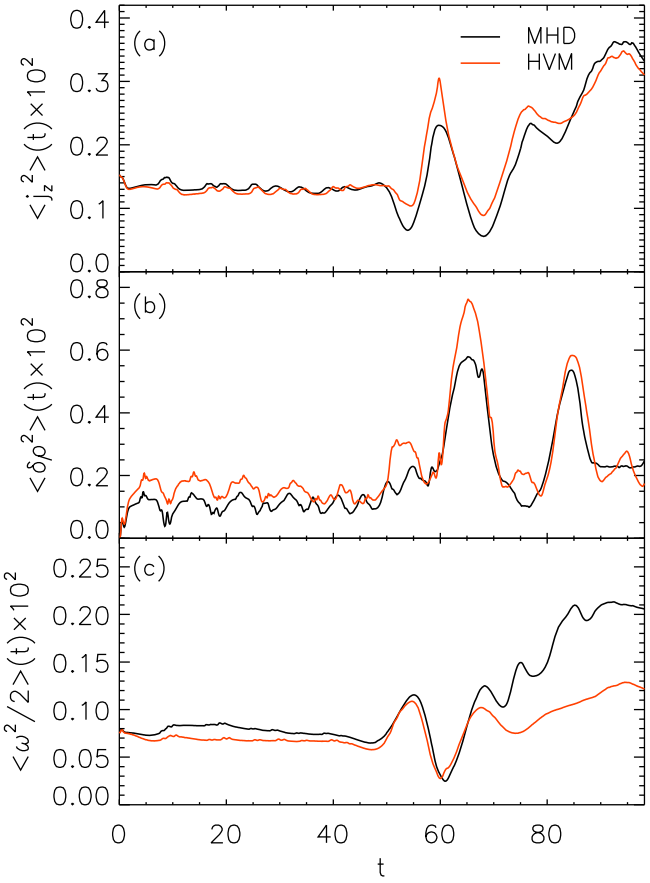

Figure 3. Temporal evolution of $\langle j_z^2 \rangle(t)$ (a), $\langle \delta\rho^2 \rangle(t)$ (b), and $\langle \boldsymbol{\omega}^2/2 \rangle(t)$ (c) for the MHD (black line) and HVM (red line) simulations.

evolution of MHD are not strong enough to break the invariance of $\sigma_c(t)$. On the other hand, the breaking of the invariance of σ_c in the Vlasov run is associated with the presence of both dispersive and kinetic effects. Indeed, evaluation of the incompressible Hall MHD invariant σ_g (generalized helicity) (Turner 1986; Servidio et al. 2008) shows that it is also not preserved for the HVM run and it shows a similar behavior to σ_c (in particular a jump is recovered at $t \simeq \tau$). This feature suggests that the production of $\sigma_c(t)$ recovered in the kinetic simulation cannot be associated only with dispersive effects, which are taken into account in the Hall model, but is also due to the presence of kinetic effects.

In contrast, the evolution of the residual energy $\sigma_r(t)$ is very similar in the MHD and HVM simulations. Referring to Figure 2(b), we see that in the initial stages $\sigma_r \simeq 0$, then it oscillates strongly during the collisions between wave packets, first to positive values indicating a positive correlation of the Elsässer fields, then more strongly toward negative values of correlation, returning to positive correlation again prior to finally approaching zero once again. It is clear that during the collision there is substantial exchange of kinetic and magnetic energy, and this is not greatly influenced by kinetic effects.

In order to compare the role of small-scale dynamics in the two cases, we computed the mean square out-of-plane electric current density $\langle j_z^2 \rangle$ as a function of time. This is illustrated in the top panel of Figure 3 for the MHD (black) and kinetic HVM (red) runs. $\langle j_z^2 \rangle(t)$ shows a similar time evolution in the two cases. In particular, both models show a peak of $\langle j_z^2 \rangle(t)$

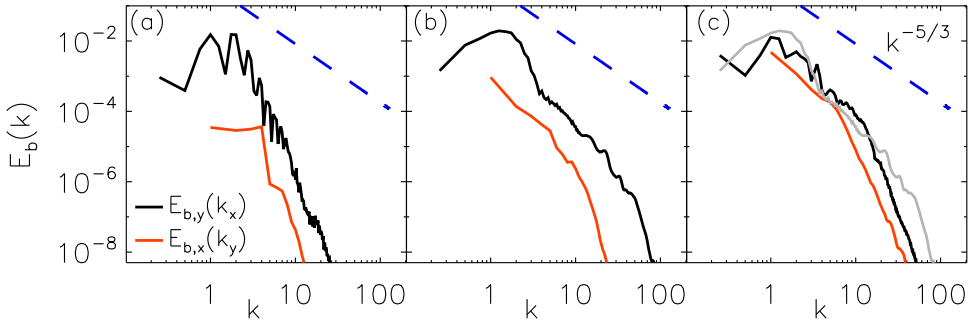

Figure 4. Power spectral density of the magnetic energy E_b at three time instants: $t = 29.4$ (a), $t = \tau = 58.9$ (b), and $t = 88.4$ (c). In each panel the black curve indicates $E_{b,y}(k_x) = \sum_{k_y} E_b(k_x, k_y)$, the red curve refers to $E_{b,x}(k_y) = \sum_{k_x} E_b(k_x, k_y)$, and the dashed blue line indicates the slope $k^{-5/3}$ as a reference. The gray line in panel (c) represents $E_{b,y}(k_x)$ at $t = 58.9$, which corresponds to the black line of panel (b).

around the collision time $t \simeq \tau$. After the collision, a high intensity of current activity persists and the peak of current activity is reached in the final stage of the simulations.

Other quantities that provide further physical details about the simulations are $\langle \delta\rho^2 \rangle$, the density fluctuations providing a measure of compressibility, and $\langle \boldsymbol{\omega}^2/2 \rangle$, the mean square vorticity or enstrophy, where $\delta\rho = \rho - \langle \rho \rangle$ and $\boldsymbol{\omega} = \boldsymbol{\nabla} \times \boldsymbol{u}$. Panels (b) and (c) of Figure 3 respectively show $\langle \delta\rho^2 \rangle$ and $\langle \boldsymbol{\omega}^2/2 \rangle$ for both simulations. The density fluctuations peak around $t \simeq 65$ and $t \simeq 85$. The first peak is due to the interaction between the two wave packets. The second peak of density fluctuations appears to be due to propagation of magnetosonic fluctuations generated by the initial strong collision. Once generated, these modes propagate across the periodic box and provide an "echo" of the original collision. We also note that $\langle \delta\rho^2 \rangle$ exhibits some small modulations in the initial stage of both simulations, which could be produced by the absence of a pressure balance in the initial condition.

The evolution of enstrophy $\langle \boldsymbol{\omega}^2/2 \rangle$, also shown in Figure 3, indicates that both MHD and HVM cases produce fine-scale structure in the velocity, i.e., vortical structures, during the collisions, and these persist after the collision. However, $\langle \boldsymbol{\omega}^2/2 \rangle$ reaches larger values in the MHD case than in the HVM case. This could be due to the presence of kinetic damping effects, which decrease the intensity of $\langle \boldsymbol{\omega}^2/2 \rangle$ by transferring energy to the VDF (see, e.g., Del Sarto et al. 2016; Parashar & Matthaeus 2016). It is interesting to note that the general profiles of enstrophy and mean square current follow similar trends in time. This can be expected because the inertial range of turbulence typically provides near-equipartition of velocity and magnetic fluctuation energy, even in fairly simple configurations (Matthaeus & Lamkin 1986). However, when examined in more detail, one often finds, as here, that the magnetic fluctuations are usually about a factor of two more energetic in the inertial range part of the spectrum, as they are, for example in the solar wind (Matthaeus & Goldstein 1982). This inequality is here reflected in the fact that $\langle j_z^2 \rangle > \langle \boldsymbol{\omega}^2/2 \rangle$.

In order to further characterize the small-scale fluctuation generated by the collisions and associated nonlinear activity, we examine the magnetic energy spectra. Figure 4 shows, for the Vlasov run, the power spectral densities of the reduced magnetic field $E_{b,y}(k_x)$ (black) and $E_{b,x}(k_y)$ (red) at (a) $t = 29.4$, (b) $t = \tau = 58.9$, and (c) $t = 88.4$. Here, for example, $E_{b,y}(k_x)$ is a one-dimensional reduced power spectral density obtained by integrating over one component of wavevector. The blue dashed lines in Figure 4 indicate a $k^{-5/3}$ slope for reference. We remark that the spectra for the HVM run show more energy at very small scales than those for the MHD run (not shown here), again consistent with the idea that the HVM run produces more fine scales than the MHD simulation. This may simply indicate that the effective dissipation in the HVM case is smaller than the numerically motivated dissipation coefficients selected for the MHD run.

In Figure 4 we observe that, at $t = 29.4$, the spectrum $E_{b,y}(k_x)$ is steep due to the localization of the initial condition, which requires the involvement of a wide range of wavenumbers k_x. Furthermore, during the evolution, the spectra show a transfer of energy toward small scales, at higher k_x and at higher k_y. This represents a signature of energy transfer due to nonlinear coupling. In fact, much of the energy $E_{b,y}(k_x)$ is contained, at $t = \tau$, in a bump around $k = 1$, while at $t = 88.4$ the bump is less clear and the spectrum $E_{b,y}(k_x)$ is more developed. A break in $E_{b,y}(k_x)$ can also be appreciated around $k_{d_p} \simeq 10$.

Another feature of the magnetic energy spectra is that $E_{b,x}(k_y)$, which initially contains less energy than $E_{b,y}(k_x)$, experiences a significant increase in power, reaching almost the same amplitude at the later times. This suggests that fluctuations become more isotropic, and that energy transfer is efficient in both directions of the wavevector space.

4. CONCLUSIONS

We have carried out a comparative study using different plasma simulation methods to examine the dynamical evolution that accompanies the interaction or collision of two oppositely propagating wave packets. For the classic case of incompressible MHD, considered by Moffatt and by Parker, the wave packets are, when considered separately, exact large-amplitude solutions of the nonlinear equations, and are therefore, strictly speaking, "waves". If two such waves, oppositely propagating, overlap then nonlinear couplings and turbulence can be produced and the packets are deformed. Moffatt and Parker concluded that, after the characteristic interaction time, the packets again separate and continue propagating away from one another without further nonlinear interactions. Hence one question addressed in the present study is whether such separation after a collision actually occurs. A second question is whether departures from incompressible MHD change the dynamics in an appreciable way. To that end, we examined here a compressible MHD formulation and a hybrid Vlasov formulation.

Our results show that—when one moves beyond the MHD framework in which the problem of Moffatt & Parker is approached—the dynamics become more complex. Here we

find that, in both the present cases, the interactions and the structures produced in the collision are sufficiently complex that it is difficult to determine whether the wave packets actually attain a full separation after the collision. Indeed, we note that very complex current and vorticity structures are produced at small scales in both compressible MHD and HVM cases, and these fluctuations are indicative of a spread of energy in the plane of the wavevectors, which is almost perpendicular to $\boldsymbol{B}_0$. The energy spectra evolve toward isotropy in this plane, although one would expect a degree of spectral anisotropy to persist due to the presence of the weak in-plane magnetic field. Furthermore, to the extent that the interaction of the packets has a finite lifetime (as envisioned, e.g., by Kraichnan 1965), any such relaxation would be expected to be incomplete in a single interaction time.

In addition, we recall that cross-helicity is conserved in the incompressible ideal problem, so that after the collision in that case, the separated wave packets will each contain the same energy as was present in the initial state. However, cross-helicity is not preserved in the kinetic case since dispersive (e.g., Hall effect) and dissipative effects are present in the simulation. In fact, in the HVM case, we observe a significant change in global cross-helicity during the interaction.

This preliminary examination of the fate of the conjecture of Moffatt and Parker in the context of compressible as well as kinetic models has produced a satisfactory, if not complete, picture. In fact, the basic physics of the collisions of large-amplitude Alfvén waves as envisioned by those authors appears to be upheld in this regime. However, we have neither examined the most general case, which would require full 3D simulations, nor completely analyzed the compressible and kinetic effects in the present cases. In particular, not shown here are indications of specific kinetic wave modes and characteristic distortions of the VDF (Servidio et al. 2015; Vásconez et al. 2015) that might be expected. A separate account of these results is in preparation. We also note that we have analyzed the present problem by employing several other models including hybrid PIC and Hall MHD, and also by varying the initial conditions. Such results are of interest in the context of, e.g., the Turbulent Dissipation Challenge (Parashar et al. 2015b) and will be reported at a later time.

Research is supported by NSF AGS-1063439, AGS-1156094 (SHINE), AGS-1460130 (SHINE), and NASA grants NNX14AI63G (Heliophysics Grandchallenge Theory), and the Solar Probe Plus science team (ISIS/SWRI subcontract No. D99031L), and Agenzia Spaziale Italiana under the contract ASI-INAF 2015-039-R.O "Missione M4 di ESA: Partecipazione Italiana alla fase di assessment della missione THOR". Kinetic numerical simulations here discussed have been run on the Fermi supercomputer at Cineca (Bologna, Italy), within the ISCRA-C project IsC37-COLALFWP (HP10CWCE72).

REFERENCES

Alexandrova, O., Carbone, V., Veltri, P., & Sorriso-Valvo, L. 2008, ApJ, 674, 1153
Armstrong, J., Cordes, J., & Rickett, B. 1981, Natur, 291, 561
Barnes, A. 1979, Space Plasma Physics: The Study of Solar-System Plasmas (Washington, DC: National Academy of Sciences)
Belcher, J. W., & Davis, L., Jr. 1971, JGR, 76, 3534
Bruno, R., Bavassano, R., & Villante, U. 1985, JGR, 90, 4373
Bruno, R., & Carbone, V. 2013, LRSP, 10, 1
Chandrasekhar, S. 1956, PNAS, 42, 273
Del Sarto, D., Pegoraro, F., & Califano, F. 2016, PhRvE, 93, 053203
Dobrowolny, M., Mangeney, A., & Veltri, P. 1980a, PhRvL, 45, 144
Dobrowolny, M., Mangeney, A., & Veltri, P. 1980b, Solar and Interplanetary Dynamics (Dordrecht: Springer)
Drake, D. J., Howes, G. G., Rhudy, J. D., et al. 2016, PhPl, 23, 022305
Elsässer, W. M. 1950, PhRv, 79, 183
Galtier, S., Nazarenko, S. V., Newell, A. C., & Poucket, A. 2000, JPlPh, 63, 447
Gary, S. P., Saito, S., & Narita, Y. 2010, ApJ, 716, 1332
He, J., Tu, C., Marsch, E., et al. 2015, ApJL, 813, L30
Hollweg, J. V. 1999, JGR, 104, 14811
Howes, G. G., & Nielson, K. D. 2013, PhPl, 20, 072302
Iroshnikov, R. S. 1964, SvA, 7, 566
Kraichnan, R. H. 1965, PhFl, 8, 1385
Kraichnan, R. H., & Montgomery, D. 1980, RPPh, 43, 547
Marsch, E. 2006, LRSP, 3, 1
Matthaeus, W. H., & Goldstein, M. L. 1982, JGR, 87, 6011
Matthaeus, W. H., & Lamkin, S. L. 1986, PhFl, 29, 2513
Matthaeus, W. H., Zank, G. P., Oughton, S., Mullan, D. J., & Dmitruk, P. 1999, ApJL, 523, L93
Matthaeus, W. H., Zank, G. P., Smith, C. W., & Oughton, S. 1999, PhRvL, 82, 3444
McComas, D. J., Barraclough, L., Funsten, H. O., et al. 2000, JGR, 105, 419
Moffatt, H. K. 1978, Field Generation in Electrically Conducting Fluids (Cambridge: Cambridge Univ. Press)
Ng, C. S., & Bhattacharjee, A. 1996, ApJ, 465, 845
Orszag, S. 1971, StAM, 50, 293
Orszag, S. A. 1977, in Fluid Dynamics: Les Houches 1973, ed. R. Balian & J. L. Peube (New York: Gordon and Breach), 237
Orszag, S. A., & Patterson, G. S. 1972, PhRvL, 28, 76
Oughton, S., Dmitruk, P., & Matthaeus, W. H. 2006, PhPl, 13, 2306
Parashar, T. N., & Matthaeus, W. H. 2016, ApJ, 832, 57
Parashar, T. N., Matthaeus, W. H., Shay, M. A., & Wan, M. 2015a, ApJ, 811, 112
Parashar, T. N., Oughton, S., Matthaeus, W. H., & Wan, M. 2016, ApJ, 824, 44
Parashar, T. N., Salem, C., Wicks, R. T., et al. 2015b, JPlPh, 81, 905810513
Parker, E. N. 1979, Cosmical Magnetic Fields: Their Origin and Their Activity (Oxford: Oxford Univ. Press)
Pucci, F., Vásconez, C. L., Pezzi, O., et al. 2016, JGR, 121, 1024
Sahraoui, F., Galtier, S., & Belmont, G. 2007, JPlPh, 73, 723
Servidio, S., Matthaeus, W. H., & Carbone, V. 2008, PhPl, 15, 042314
Servidio, S., Valentini, F., Califano, F., & Veltri, P. 2012, PhRvL, 108, 045001
Servidio, S., Valentini, F., Perrone, D., et al. 2015, JPlPh, 81, 325810107
Turner, L. 1986, ITPS, 14, 849
Valentini, F., Servidio, S., Perrone, D., et al. 2014, PhPl, 21, 082307
Valentini, F., Travnicek, P., Califano, F., Hellinger, P., & Mangeney, A. 2007, JCoPh, 225, 753
Vásconez, C. L., Pucci, F., Valentini, F., et al. 2015, ApJ, 815, 7
Velli, M., Grappin, R., & Mangeney, A. 1989, PhRvL, 63, 1807
Verdini, A., Velli, M., & Buchlin, E. 2009, ApJL, 700, L39
Zank, G. P., & Matthaeus, W. H. 1992, JGR, 97, 189